DOI: 10.1002/2016GL072241

AGU PUBLICATIONS

Geophysical Research Letters

RESEARCH LETTER
10.1002/2016GL072241

Key Points:
- We use a coupled climate model to investigate the effects of sulfate aerosols and carbon dioxide from the Chicxulub impact
- We find severe cooling suggesting a major role of the impact in the mass extinction event
- Surface cooling of the ocean results in vigorous mixing which could have caused a plankton bloom

Correspondence to:
J. Brugger and G. Feulner,
brugger@pik-potsdam.de;
feulner@pik-potsdam.de

Citation:
Brugger, J., G. Feulner, and S. Petri (2017), Baby, it's cold outside: Climate model simulations of the effects of the asteroid impact at the end of the Cretaceous, *Geophys. Res. Lett.*, *44*, 419–427, doi:10.1002/2016GL072241.

Received 27 OCT 2016
Accepted 18 DEC 2016
Accepted article online 20 DEC 2016
Published online 13 JAN 2017

Baby, it's cold outside: Climate model simulations of the effects of the asteroid impact at the end of the Cretaceous

Julia Brugger[1,2,3], Georg Feulner[1,3], and Stefan Petri[1]

[1]Earth System Analysis, Potsdam Institute for Climate Impact Research, Potsdam, Germany, [2]Institut für Physik und Astronomie, Universität Potsdam, Potsdam, Germany, [3]Berlin-Brandenburg Institute of Advanced Biodiversity Research, Berlin, Germany

Abstract Sixty-six million years ago, the end-Cretaceous mass extinction ended the reign of the dinosaurs. Flood basalt eruptions and an asteroid impact are widely discussed causes, yet their contributions remain debated. Modeling the environmental changes after the Chicxulub impact can shed light on this question. Existing studies, however, focused on the effect of dust or used one-dimensional, noncoupled atmosphere models. Here we explore the longer-lasting cooling due to sulfate aerosols using a coupled climate model. Depending on aerosol stratospheric residence time, global annual mean surface air temperature decreased by at least 26°C, with 3 to 16 years subfreezing temperatures and a recovery time larger than 30 years. The surface cooling triggered vigorous ocean mixing which could have resulted in a plankton bloom due to upwelling of nutrients. These dramatic environmental changes suggest a pivotal role of the impact in the end-Cretaceous extinction.

1. Introduction

During the mass extinction at the Cretaceous-Paleogene boundary, a substantial number of biological groups experienced major extinctions, including nonavian dinosaurs, other vertebrates, marine reptiles and invertebrates, planktonic foraminifera, and ammonites [*Bambach*, 2006]. The severity of this event, recently dated at 66.043 ± 0.043 Ma [*Renne et al.*, 2013], and the fact that it marks the demise of the dinosaurs account for the continued interest in understanding its origin. Yet the ultimate cause of the end-Cretaceous extinction remains debated. Most investigations today focus on two theories based on events roughly coinciding with the extinction: On the one hand, large-scale volcanic eruptions occurred around that time, with the main phase of the eruptions lasting from 66.3 to 65.5 Ma [*Schoene et al.*, 2015] as documented in the flood basalts from the Deccan plateau (India). These eruptions released sulfur dioxide and carbon dioxide leading to climatic changes which could have induced the mass extinction. On the other hand, the impact of an asteroid resulting in the Chicxulub crater (Mexico), dated to coincide with the extinction event within the errors [*Renne et al.*, 2013], resulted in dramatic local and short-term consequences but would also have produced large amounts of dust, sulfate aerosols, and greenhouse gases which affected the climate globally and on longer timescales [*Kring*, 2007; *Schulte et al.*, 2010]. In addition to improvements in sampling and dating the geological and paleontological record, modeling studies of the environmental changes associated with these events can help to assess competing theories [*Feulner*, 2009]. In this paper, we use coupled climate model simulations to explore the effects of the Chicxulub impact on Earth's climate.

The initial impact hypothesis proposed that dust particles produced during the impact were responsible for shutting down photosynthesis after the impact [*Alvarez et al.*, 1980]. Early modeling studies investigating the climate changes associated with the Chicxulub impact therefore mostly focused on these effects [e.g., *Covey et al.*, 1994]. More recent studies of the debris in the impact layer suggest, however, that the fraction of submicron-sized dust particles in the stratosphere was too small to cause the observed environmental changes [*Pope*, 2002]. Instead, the production of sulfur-bearing gases from the impact target's evaporites is considered the key source of climatic effects, as they form stratospheric sulfate aerosols which block sunlight and thus cool down the Earth's atmosphere and hamper photosynthesis [*Pierazzo et al.*, 1998]. The few existing studies focusing on the aerosols' effect used noncoupled climate models [*Pope et al.*, 1994, 1997; *Pierazzo et al.*, 2003] and are limited to short time periods after the impact without investigating the longer-term changes.

Here we use a coupled climate model [*Montoya et al.*, 2005]—consisting of an ocean general circulation model, a fast atmosphere, and a dynamic/thermodynamic sea ice model—to explore the climatic effects of sulfate aerosols and CO_2 following the impact. We explicitly focus on global and longer-term changes and do not consider local and short-term phenomena like the extreme heat, strong winds, wildfires, and tsunamis close to the impact site [*Kring*, 2007].

2. Modeling Setup

2.1. Preimpact Climate Model Simulations

The simulations of the end-Cretaceous climate and the effects of the impact are carried out with a coupled climate model [*Montoya et al.*, 2005] consisting of a modified version of the ocean general circulation model MOM3 [*Pacanowski and Griffies*, 1999; *Hofmann and Morales Maqueda*, 2006] run at a horizontal resolution of 3.75° × 3.75° with 24 vertical levels, a dynamic/thermodynamic sea ice model [*Fichefet and Maqueda*, 1997], and a fast statistical-dynamical atmosphere model [*Petoukhov et al.*, 2000] with a coarse resolution of 22.5° in longitude and 7.5° in latitude.

Our impact simulations are based on a climate simulation of the end-Cretaceous climate state using a Maastrichtian (70 Ma) continental configuration [*Sewall et al.*, 2007]. The solar constant is scaled to 1354 W/m^2, based on the present-day solar constant of 1361 W/m^2 [*Kopp and Lean*, 2011] and a standard solar model [*Bahcall et al.*, 2001]. Orbital parameters are idealized with a circular orbit and an obliquity of 23.5°. Proxy estimates for the atmospheric CO_2 concentration range from 500 ppm to 1500 ppm for the Late Cretaceous [*Royer*, 2006]; during the period directly preceding the impact it was likely below 800 ppm [*Hong and Lee*, 2012; *Royer et al.*, 2012]. We have therefore performed a baseline simulation with 500 ppm of atmospheric CO_2 and a sensitivity experiment at a higher CO_2 concentration of 1000 ppm. Both preimpact simulations are integrated for about 2200 model years until climate equilibrium is approached.

The simulated global annual mean surface air temperature during the latest Cretaceous is 18.9°C or about 4°C above preindustrial temperatures for the 500 ppm simulation and 21.6°C or roughly 7°C warmer than the preindustrial climate for the 1000 ppm model experiment.

2.2. Modeling the Effects of the Impact

To model the climatic effects of the impact, we use literature information from geophysical impact modeling indicating that for a 2.9 km thick target region consisting of 30% evaporites and 70% water-saturated carbonates, a dunite projectile with 50% porosity, a velocity of 20 km/s, and a diameter between 15 and 20 km, a sulfur mass of 100 Gt is produced [*Pierazzo et al.*, 1998]. For comparison, this corresponds to about 10,000 times the amount of sulfur released during the 1991 Pinatubo eruption [*McCormick et al.*, 1995]. Note that the amount of sulfur released during the impact depends on the composition of the targeted bedrock, vaporization criteria, the condensation of vaporized ejecta, possible back reactions, and the impactor's velocity and size [*Pierazzo et al.*, 1998; *Gupta et al.*, 2001]. However, the results do not strongly depend on the precise amount of sulfur released during the impact, since the radiative forcing does not increase for sulfur masses larger than 30 Gt [*Pierazzo et al.*, 2003].

The effects of the stratospheric sulfate aerosols on radiation are based on a simple sulfate aerosol model coupled to a column radiation model [*Pierazzo et al.*, 2003]. Sulfur is assumed to be ligated in the forms of SO_2 (80%) and SO_3 (20%). The ratio of SO_3 to SO_2 determines the amount of stratospheric sulfate aerosols formed and their concentration with time. *Ohno et al.* [2014] suggest a SO_3/SO_2 ratio of 100/1 , which implies a higher initial sulfate aerosol concentration but faster decay. Compared to the ratio used in our study, this would lead to a slightly faster decay of stratospheric aerosols [*Pierazzo et al.*, 2003]. Only the aerosols in the stratosphere are considered because aerosols are quickly washed out as soon as they enter the troposphere. The stratospheric residence time of tracers in a present-day steady state atmosphere is about 2 years [*Holton et al.*, 1995]. We follow *Pierazzo et al.* [2003] and include the effect of a possible longer residence time in a perturbed atmosphere after the impact by simulating the effects of the impact for 2.1, 4.3, and 10.6 years stratospheric residence time.

To model the time after the impact, we use time sequences of visible transmission taken from *Pierazzo et al.* [2003] for the different stratospheric residence times discussed above. With this model setup, solar flux at the surface is drastically reduced immediately after the impact from a preimpact value of 169.5 W/m^2 to the minimum value of 2.28 W/m^2 for 2.1 years stratospheric residence time, reached in the first year after the impact,

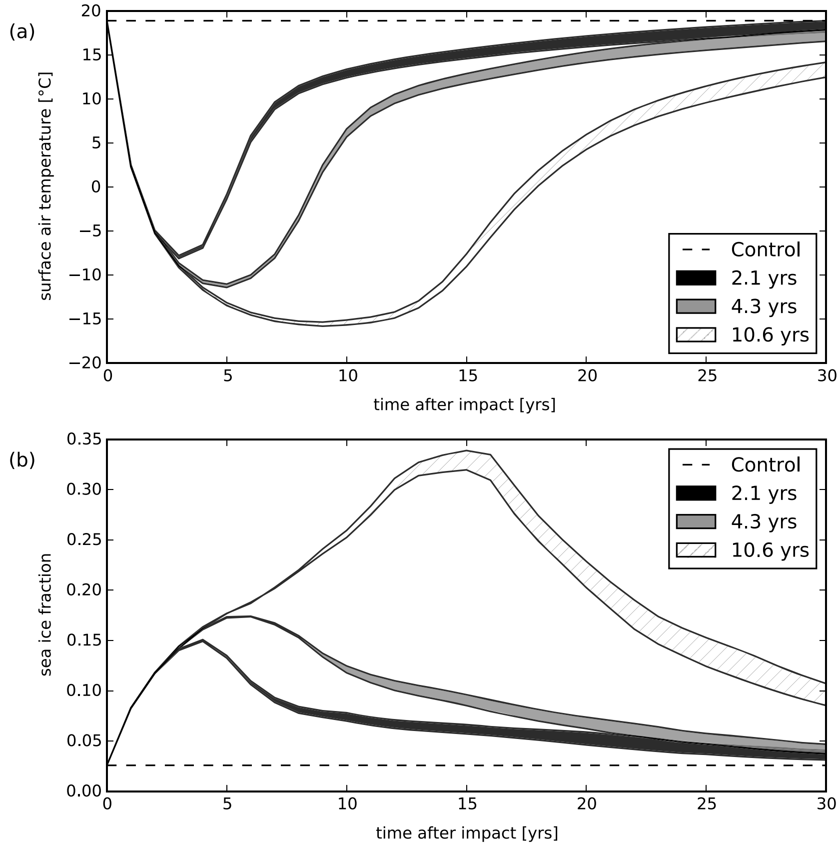

Figure 1. (a) Simulated global annual mean surface air temperature and (b) global sea ice fraction during the 30 years after the impact for the baseline state with 500 ppm of carbon dioxide and for the three different stratospheric aerosol residence times. For each residence time, the shaded region marks the uncertainty due to the carbon dioxide released from the impact alone and from the impact and the biosphere, respectively, ranging from 180 ppm to 540 ppm.

and 2.03 W/m^2 for 4.3 and 10.6 years stratospheric residence time, reached in the second year after the impact. Stratospheric residence time does not strongly influence minimum solar flux but rather determines the time needed to regain the preimpact value which is reached after 6, 10, and 20 years for the different residence times.

In addition to the sulfate aerosols' effect, we consider an enhanced CO_2 concentration due to the impact. For a sulfur mass of 100 Gt, about 1400 Gt of carbon dioxide is injected into the atmosphere [*Pierazzo et al.*, 1998], corresponding to an increase of the atmospheric CO_2 concentration by 180 ppm. Note that the amount of CO_2 released from the impact depends on the energy and angle of the impact, the fractions of carbonates in the impactor, and the target as well as the recombination rate [*O'Keefe and Ahrens*, 1989; *Pierazzo et al.*, 1998]. Moreover, there could be additional CO_2 emissions from ocean outgassing and perturbations of the terrestrial biosphere, so we run additional simulation experiments adding a total of 360 ppm and 540 ppm of CO_2 as sensitivity experiments. Both sulfate aerosols and CO_2 produced during the impact event are assumed to be distributed globally and uniformly in our model simulations. A uniform aerosol distribution is a simplification but may be a reasonable approximation given the magnitude and location of the Chicxulub impact. We assume that the shorter-term effects of dust are overshadowed by the aerosol effect. Furthermore, we neglect water vapor as the amount produced is uncertain and its tropospheric residence time is very short. Finally, we do not consider the climatic consequences of ozone destruction after the impact [*Kring*, 2007] since they are probably of minor importance for the global climate. All impact experiments are performed for both end-Cretaceous climate states with 500 ppm and 1000 ppm of atmospheric CO_2 and are integrated for 100 years after the impact; the impact simulations for 2.1 years residence time are run for 1000 years.

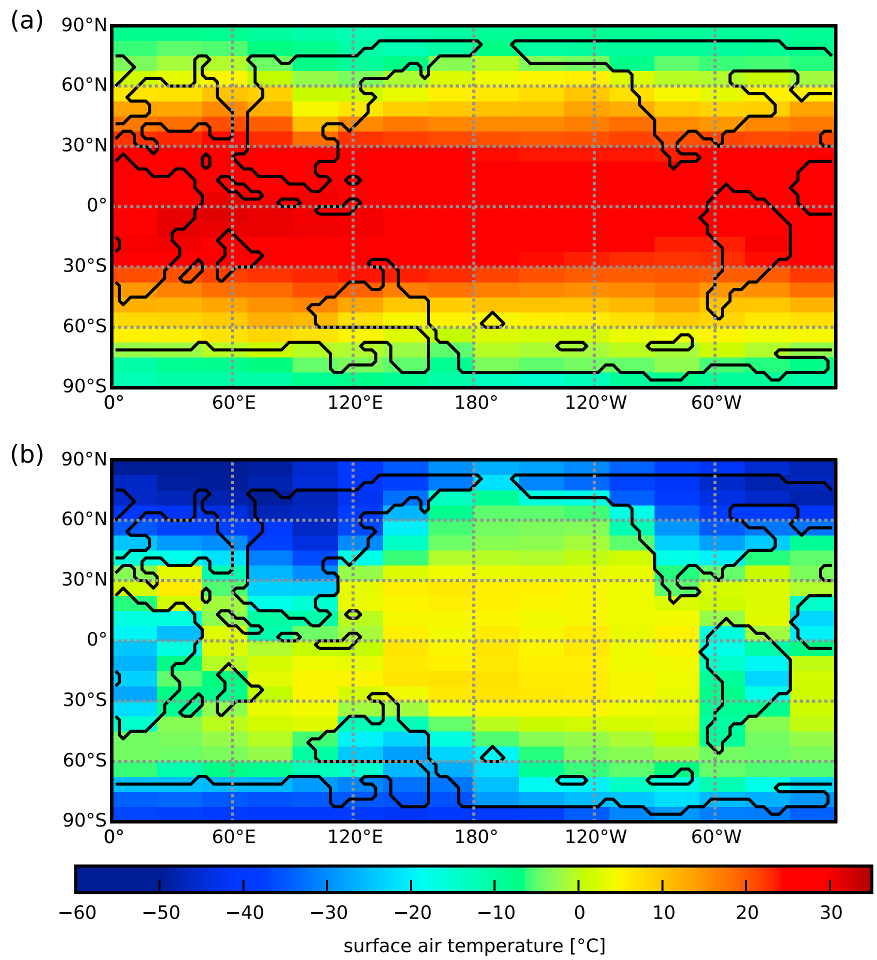

Figure 2. Map of annual simulated mean surface air temperature (a) before the impact and (b) for the coldest year after the impact for the baseline climate state with 500 ppm of carbon dioxide, a stratospheric residence time of 2.1 years, and additional carbon dioxide emissions of 360 ppm.

3. Results

3.1. Global Cooling

The main result from our climate model simulations is a severe and persistent global cooling in the decades after the impact. Figure 1a shows global annual mean surface air temperature during the 30 years following the impact for an atmospheric CO_2 concentration of 500 ppm before the impact, for the different aerosol residence times and for different CO_2 emission values from the impact. The temperature evolution for the different CO_2 emissions resulting from the impact is very similar; in the following, the discussion will focus on the simulation representing the intermediate emission value of 360 ppm.

For 2.1 years stratospheric residence time, which is the most conservative assumption for the simulations, global annual mean surface air temperature is reduced by 27°C when minimum temperature is reached in year 3 after the impact. This temperature difference is not sensitive to the CO_2 concentration before the impact: in the case of a preimpact concentration of 1000 ppm, the temperature drops by an almost identical amount from +22°C to −5.0°C. Global annual mean surface air temperature remains below freezing for 3 years. For 4.3 years and 10.6 years stratospheric residence time, minimum global annual mean surface air temperature is even lower (cooling by 30°C and 34°C) and reached at later times (years 5 and 9 after the impact). In these simulations with longer residence times, global annual mean subfreezing temperatures persist for 7 and 16 years, respectively. The drastic and prolonged cooling in particular in the 10.6 years residence time scenario raises the question, however, whether longer stratospheric residence times can really be reconciled with the paleontological record, in particular with the observed fast recovery of productivity [*D'Hondt et al.*, 1998;

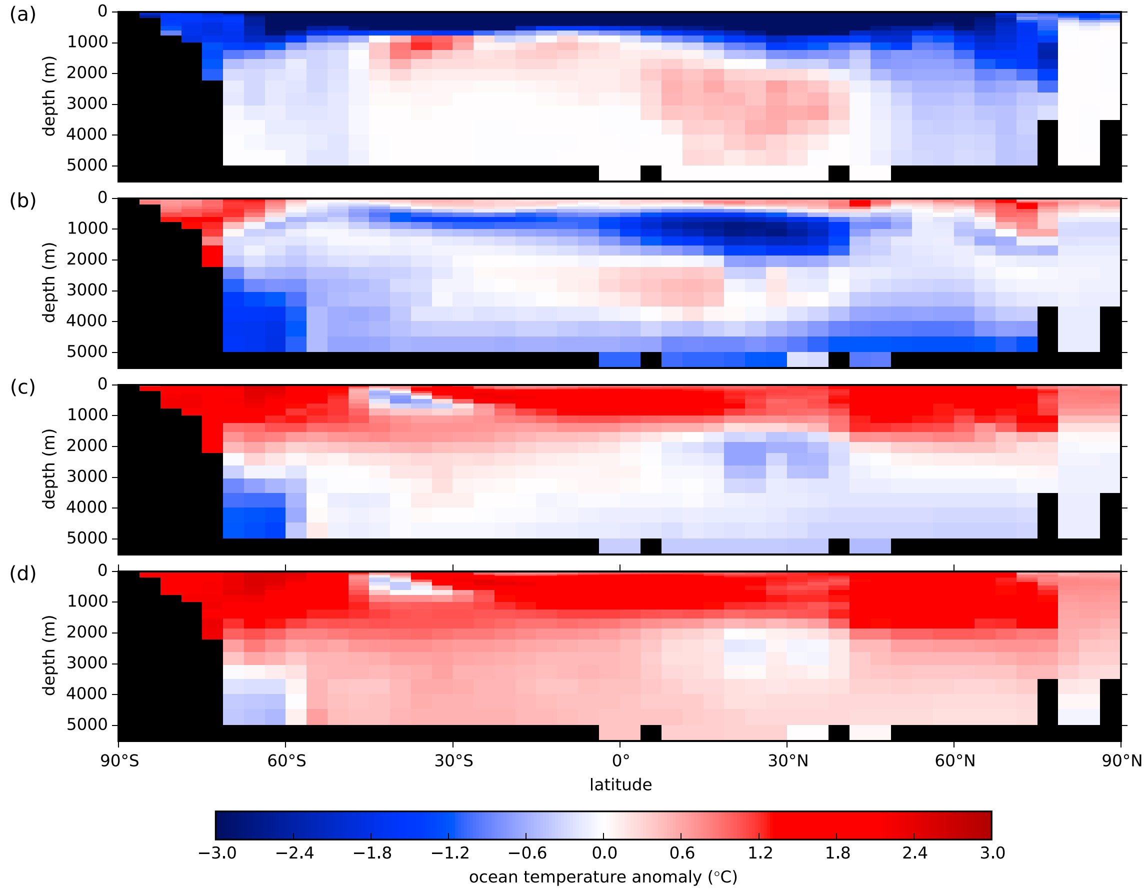

Figure 3. Meridional profiles of ocean temperature anomalies relative to the control run (a) 3 years, (b) 100 years, (c) 500 years, and (d) 1000 years after the impact. The range of the color bar has been chosen to emphasize anomalies on longer timescales; the near-surface cooling in Figure 3a therefore exceeds this range.

Alegret et al., 2012; *Sepúlveda et al.*, 2009]. In the following, we focus on the simulations with 2.1 years stratospheric residence time of the aerosols, representing the most conservative case.

The postimpact cooling observed in our simulations is accompanied by a marked expansion of snow and sea ice. Annual average surface albedo increases from 0.11 before the impact to 0.24 in the year with maximum ice cover in our standard simulation (500 ppm CO_2 preceding the impact, 2.1 years residence time, and 360 ppm CO_2 from the impact). As an example for this expansion of snow and ice, Figure 1b shows the time evolution of the global sea ice fraction during the three decades after the impact. For our standard case of 2.1 years stratospheric aerosol residence time, the sea ice fraction increases by a factor of 6 before declining toward its preimpact value. Interestingly, the simulation with 10.6 years residence time exhibits a distinctly different behavior. In this case, the sea ice fraction strongly increases after the initial cooling period, indicating the beginning of a runaway caused by the positive ice-albedo feedback. This runaway is eventually slowed and reversed by the increasing solar radiation, however. For the other residence times, the reduction of solar radiation due to the impact is too short to initiate this process. This also means, however, that a perturbation with an even longer residence time might be sufficient to trigger a snowball runaway.

We note that the emission of CO_2 from the impact will lead to warming compared to the preimpact state after the initial cooling period. Depending on the amount of CO_2 emitted from the impact, after 1000 years the climate is 1.0–2.6°C warmer than the preimpact state for an initial CO_2 concentration of 500 ppm and 0.5–1.4°C warmer for 1000 ppm.

3.2. Regional Cooling

Regional temperature changes induced by the asteroid impact are even more severe than suggested by the global averages. Maps of surface air temperature of the preimpact year and the year of minimum global annual mean temperature indicate pronounced regional cooling, in particular over continental areas and in

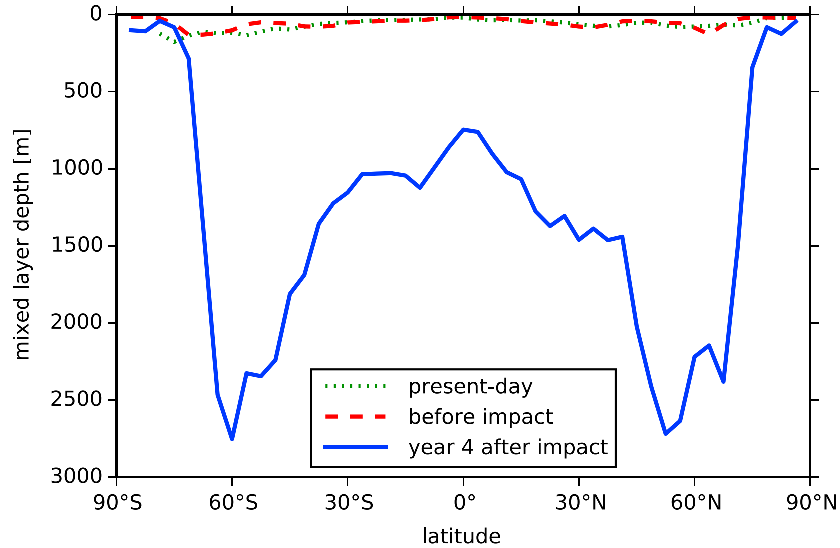

Figure 4. Ocean mixed-layer depth before the impact and in the coldest year for the baseline simulation with 500 ppm of carbon dioxide, 2.1 years residence time, and 360 ppm of carbon dioxide from the impact. The present-day mixed-layer depth from a simulation for the end of the twentieth century [*Feulner*, 2011] is shown for comparison.

polar regions (see, e.g., Figure 2, for 500 ppm of CO_2 preceding the impact, 2.1 years stratospheric residence time, and 360 ppm of CO_2 from the impact). Global annual mean temperatures over land fall to −32°C in the coldest year (compared to +15°C before the impact), with continental temperatures in the tropics reaching a mere −22°C (falling from +27°C before the impact). In contrast, global mean sea surface temperatures drop to +5.9°C only from their preimpact value of +21°C. We note that our model shows an enhanced land-ocean warming ratio of ∼2 in the tropics for idealized CO_2 increase scenarios [*Eby et al.*, 2013] as compared to a ratio of ∼1.3 in other models [*Schmidt et al.*, 2014]. The cooling over land after the Chicxulub impact may therefore be overestimated in our model.

3.3. Deep-Ocean Temperature and Mixing

Because of the ocean's thermal inertia, surface temperature changes propagate only slowly into the deep ocean. It is therefore interesting to investigate longer-term temperature changes in the deep ocean. Figure 3 shows meridional profiles of ocean temperature changes for four time slices up to 1000 years after the impact. In year 3 after the impact, the strong surface cooling results in very cold water masses in the upper ∼1000 m of the ocean at all latitudes and down to the ocean floor at high latitudes. One hundred years after the impact near-surface ocean layers show evidence of warming due to the CO_2 released after the impact, while the cold water masses have reached the abyss, with pronounced cooling in the deep ocean at high latitudes. The most striking feature at this point of time, however, is a bubble of cold water at depths of ∼500–2000 m which is particularly pronounced in the northern tropics and subtropics. Regionally, this bubble is located in the northern Atlantic (not shown). After 500 years, the situation is characterized by warmer waters in the upper half of the ocean and slightly cooler water persisting in the deep ocean. The cold bubble has weakened and is restricted to the northern subtropics and to depths of ∼2000–3000 m. One thousand years after the impact, warming has reached the deep ocean, with only few localized regions of minor cooling persisting in the abyss of the Southern Ocean and in the northern subtropics.

Finally, we will explore how the cooling due to the Chicxulub impact affects ocean mixing and potentially the marine biosphere. Figure 4 shows the mixed-layer depth before the impact and in the coldest year after the event. In the Late Cretaceous climate preceding the impact, the mixed-layer depth is comparable to a simulation of the present-day climate state. This changes dramatically after the impact. The sudden atmospheric cooling triggered by the impact leads to strongly enhanced ocean mixing and deep water formation notably at midlatitudes. The collapsed ^{13}C gradient observed at the Cretaceous-Paleogene boundary could provide geologic evidence for this mixing [*Zachos et al.*, 1989], although a decrease in marine productivity might have contributed to the changes in ^{13}C as well. The vigorous ocean mixing after the impact will transport nutrients from the deep ocean toward the surface. We argue that the increase in available nutrients should result in a pronounced rise of ocean primary production following the initial decrease due to the darkness after the impact. Additional nutrients from impact ejecta [*Parkos et al.*, 2015] could further intensify ocean primary productivity. Depending on the availability of light and limiting nutrients like iron, this could result in regional plankton blooms, as proposed by geologic explorations [*Hollis et al.*, 1995]. The plankton blooms could also have created toxins with profound effects on marine near-surface ecosystems [*Wilde and Berry*, 1986; *Castle and Rodgers*, 2009]. This scenario would have to be further explored with a model for the marine biogeochemistry.

4. Discussion

In this section, we briefly compare our results with earlier modeling work and proxy evidence. Comparable modeling studies considering the aerosols' effect and using coupled climate models do not exist. *Pope et al.* [1997] use a radiative-transfer model to roughly estimate the global cooling from sulfate aerosols, finding values similar to the ones reported here. With respect to proxy data, it is difficult to compare the cooling found in our simulations because a very high time resolution is necessary to record the fast climatic changes associated with the impact. Furthermore, the prominent proxy carriers for the surface ocean, calcareous microfossils, suffered from the extinction.

However, two recent studies [*Vellekoop et al.*, 2014, 2016] use TEX_{86} paleothermometry of shallow marine sediments to estimate sea surface temperature changes across the Cretaceous-Paleogene boundary. From the Brazos River section (Texas), *Vellekoop et al.* [2014] reconstruct preimpact temperatures of 30–31°C in good agreement with the tropical Late Cretaceous sea surface temperature from well-preserved foraminifer shells [*Pearson et al.*, 2001]. For comparison, the preimpact annual mean sea surface temperature of 24°C in this region in our simulation is somewhat lower. At the boundary, *Vellekoop et al.* [2014] report a drop in sea surface temperature in the Gulf of Mexico of up to 7°C lasting for months to decades but not longer than 100 years. Averaged over the decade after the impact, the sea surface temperature drops by 10°C, in good agreement with the proxy study, assuming that the resolution of their record is about a decade. *Vellekoop et al.* [2014] also report an increase in ocean temperatures by 1–2°C after the impact cooling, in agreement with the warming seen in our simulations due to the additional CO_2 released from the impact. *Vellekoop et al.* [2016] use TEX_{86} data extracted from cores from the New Jersey paleoshelf to reconstruct temperatures of ∼26°C at the end of the Cretaceous as well as an abrupt ∼3°C cooling at the boundary to the Paleogene. As for the Texas record, our preimpact temperature of ∼19°C is lower than the TEX_{86} estimate; however, our cooling of ∼9°C is more pronounced than the proxy signal at this location.

It should be kept in mind, however, that a detailed comparison of local proxy records is hampered by the comparatively coarse spatial resolution of our model as well as uncertainties concerning the temporal resolution [*Vellekoop et al.*, 2016] and calibration [*Ho and Laepple*, 2016] of TEX_{86} temperature estimates.

For some locations, proxies document local cooling persisting for longer timescales of millennia. *Galeotti et al.* [2004] analyze records of dinoflagellate cysts and benthic foraminifera across the Cretaceous-Paleogene boundary in the Tunisian shelf region and present evidence for millennial-scale cooling indicated by a brief expansion of boreal species into the western Tethys Ocean. Similarly, *Vellekoop et al.* [2015] report repeated cooling pulses in this region during the first thousands of years after the impact. *Galeotti et al.* [2004] use energy balance estimates and one idealized simulation with a coupled atmosphere-ocean model under present-day boundary conditions to explore the ocean response timescale to different levels of impact aerosol cooling and interpret the millennial-scale cooling as evidence for persisting cool water masses in the deep ocean. Cooling pulses on the Tunisian shelf could then be explained by local upwelling of cold water [*Vellekoop et al.*, 2015]. The bubble of cooler ocean water in the Northern Atlantic region found in our simulations supports this notion, although the cooler water masses do not persist for more than one millennium in our simulations, mostly due to the warming from the CO_2 released during the impact.

5. Conclusions

In summary, our climate-modeling study demonstrates severe cooling and vigorous ocean mixing in the wake of the Chicxulub impact. These results are in general agreement with proxy data, but a detailed comparison is hampered by the time resolution of empirical records, questions of temperature proxy calibration, and the low spatial resolution of our model. Although we cannot conclude from our model results that the impact was exclusively responsible for the mass extinction at the end of the Cretaceous, the dramatic reduction in temperature and the expected profound perturbation of the marine biosphere due to the change in ocean circulation in our simulations certainly suggest a key role of the impact in the extinction event. The Chicxulub impact and the Deccan Trap volcanism might also have acted in concert, of course, either by the impact triggering more intense eruptions as recently argued [*Renne et al.*, 2015] or by delivering the final blow to a biosphere already stressed by the effects of the eruptions [*White and Saunders*, 2005; *Arens and West*, 2008; *Renne et al.*, 2013]. Future modeling studies will have to explore the interaction between these two causes as well as the effects on Earth's marine and terrestrial biosphere in more detail.

Acknowledgments
The authors would like to thank A. Brugger, M. Hofmann, W. Kießling, T. Laepple, W. Lucht, R. Luther, W. von Bloh, and K. Wünnemann for discussions and J. Sewall for providing Cretaceous boundary conditions. The authors gratefully acknowledge the European Regional Development Fund (ERDF), the German Federal Ministry of Education and Research, and the Land Brandenburg for supporting this project by providing resources on the high-performance computer system at the Potsdam Institute for Climate Impact Research. The work was partly funded by the German Federal Ministry of Education and Research BMBF within the Collaborative Project "Bridging in Biodiversity Science—BIBS" (funding 01LC1501A-H). The source code for the model used in this study, the data and input files necessary to reproduce the experiments, and model output data are available from the authors upon request (brugger@pik-potsdam.de, feulner@pik-potsdam.de). All data are archived at the Potsdam Institute for Climate Impact Research (PIK).

References

Alegret, L., E. Thomas, and K. C. Lohmann (2012), End-Cretaceous marine mass extinction not caused by productivity collapse, *Proc. Natl. Acad. Sci. U.S.A.*, *109*, 728–732, doi:10.1073/pnas.1110601109.

Alvarez, L. W., W. Alvarez, F. Asaro, and H. V. Michel (1980), Extraterrestrial cause for the Cretaceous-Tertiary extinction, *Science*, *208*(4448), 1095–1108, doi:10.1126/science.208.4448.1095.

Arens, N. C., and I. D. West (2008), Press-pulse: A general theory of mass extinction?, *Paleobiology*, *34*(4), 456–471, doi:10.1666/07034.1.

Bahcall, J. N., M. H. Pinsonneault, and S. Basu (2001), Solar models: Current epoch and time dependences, neutrinos, and helioseismological properties, *Astrophys. J.*, *555*(2), 990–1012, doi:10.1086/321493.

Bambach, R. K. (2006), Phanerozoic biodiversity mass extinctions, *Annu. Rev. Earth Planet. Sci.*, *34*, 127–155, doi:10.1146/annurev.earth.33.092203.122654.

Castle, J. W., and J. H. Rodgers Jr. (2009), Hypothesis for the role of toxin-producing algae in Phanerozoic mass extinctions based on evidence from the geologic record and modern environments, *Environ. Geosci.*, *16*, 1–23, doi:10.1306/eg.08110808003.

Covey, C., S. L. Thompson, P. R. Weissman, and M. C. MacCracken (1994), Global climatic effects of atmospheric dust from an asteroid or comet impact on Earth, *Global Planet. Change*, *9*(3–4), 263–273, doi:10.1016/0921-8181(94)90020-5.

D'Hondt, S., P. Donaghay, J. C. Zachos, D. Luttenberg, and M. Lindinger (1998), Organic carbon fluxes and ecological recovery from the Cretaceous-Tertiary mass extinction, *Science*, *282*, 276–279, doi:10.1126/science.282.5387.276.

Eby, M., et al. (2013), Historical and idealized climate model experiments: An intercomparison of Earth system models of intermediate complexity, *Clim. Past*, *9*, 1111–1140, doi:10.5194/cp-9-1111-2013.

Feulner, G. (2009), Climate-modelling of mass-extinction events: A review, *Int. J. Astrobiol.*, *8*, 207–212, doi:10.1017/S1473550409990061.

Feulner, G. (2011), Are the most recent estimates for Maunder Minimum solar irradiance in agreement with temperature reconstructions?, *Geophys. Res. Lett.*, *38*, L16706, doi:10.1029/2011GL048529.

Fichefet, T., and M. A. M. Maqueda (1997), Sensitivity of a global sea ice model to the treatment of ice thermodynamics and dynamics, *J. Geophys. Res.*, *102*(C6), 12,609–12,646, doi:10.1029/97JC00480.

Galeotti, S., H. Brinkhuis, and M. Huber (2004), Records of post Cretaceous-Tertiary boundary millennial-scale cooling from the western Tethys: A smoking gun for the impact-winter hypothesis?, *Geology*, *32*, 529–532, doi:10.1130/G20439.1.

Gupta, S. C., T. J. Ahrens, and W. Yang (2001), Shock-induced vaporization of anhydrite and global cooling from the K/T impact, *Earth Planet. Sci. Lett.*, *188*, 399–412, doi:10.1016/S0012-821X(01)00327-2.

Ho, S. L., and T. Laepple (2016), Flat meridional temperature gradient in the early eocene in the subsurface rather than surface ocean, *Nat. Geosci.*, *9*(8), 606–610, doi:10.1038/ngeo2763.

Hofmann, M., and M. A. Morales Maqueda (2006), Performance of a second-order moments advection scheme in an Ocean General Circulation Model, *J. Geophys. Res.*, *111*, C05006, doi:10.1029/2005JC003279.

Hollis, C. J., K. A. Rodgers, and R. J. Parker (1995), Siliceous plankton bloom in the earliest Tertiary of Marlborough, New Zealand, *Geology*, *23*(9), 835–838, doi:10.1130/0091-7613(1995)023<0835:SPBITE>2.3.CO;2.

Holton, J. R., P. H. Haynes, M. E. McIntyre, A. R. Douglass, R. B. Rood, and L. Pfister (1995), Stratosphere-troposphere exchange, *Rev. Geophys.*, *33*, 403–439, doi:10.1029/95RG02097.

Hong, S. K., and Y. I. Lee (2012), Evaluation of atmospheric carbon dioxide concentrations during the Cretaceous, *Earth Planet. Sci. Lett.*, *327*, 23–28, doi:10.1016/j.epsl.2012.01.014.

Kopp, G., and J. L. Lean (2011), A new, lower value of total solar irradiance: Evidence and climate significance, *Geophys. Res. Lett.*, *38*, L01706, doi:10.1029/2010GL045777.

Kring, D. A. (2007), The Chicxulub impact event and its environmental consequences at the Cretaceous-Tertiary boundary, *Palaeogeogr. Palaeoclimatol. Palaeoecol.*, *255*(1–2), 4–21, doi:10.1016/j.palaeo.2007.02.037.

McCormick, M. P., L. W. Thomason, and C. R. Trepte (1995), Atmospheric effects of the Mt Pinatubo eruption, *Nature*, *373*, 399–404, doi:10.1038/373399a0.

Montoya, M., A. Griesel, A. Levermann, J. Mignot, M. Hofmann, A. Ganopolski, and S. Rahmstorf (2005), The Earth system model of intermediate complexity CLIMBER-3. Part I: Description and performance for present-day conditions, *Clim. Dyn.*, *25*(2–3), 237–263, doi:10.1007/s00382-005-0044-1.

Ohno, S., et al. (2014), Production of sulphate-rich vapour during the Chicxulub impact and implications for ocean acidification, *Nat. Geosci.*, *7*, 279–282, doi:10.1038/ngeo2095.

O'Keefe, J. D., and T. J. Ahrens (1989), Impact production of CO_2 by the Cretaceous/Tertiary extinction bolide and the resultant heating of the Earth, *Nature*, *338*, 247–249, doi:10.1038/338247a0.

Pacanowski, R. C., and S. M. Griffies, (1999), The MOM-3 manual, Tech. Rep. 4, GFDL Ocean Group, NOAA/Geophys. Fluid Dyn. Lab., Princeton, New Jersey.

Parkos, D., A. Alexeenko, M. Kulakhmetov, B. C. Johnson, and H. J. Melosh (2015), NO_x production and rainout from Chicxulub impact ejecta reentry, *J. Geophys. Res. Planets*, *120*, 2152–2168, doi:10.1002/2015JE004857.

Pearson, P. N., P. W. Ditchfield, J. Singano, K. G. Harcourt-Brown, C. J. Nicholas, R. K. Olsson, N. J. Shackleton, and M. A. Hall (2001), Warm tropical sea surface temperatures in the Late Cretaceous and Eocene epochs, *Nature*, *413*(6855), 481–487, doi:10.1038/35097000.

Petoukhov, V., A. Ganopolski, V. Brovkin, M. Claussen, A. Eliseev, C. Kubatzki, and S. Rahmstorf (2000), CLIMBER-2: A climate system model of intermediate complexity. Part I: Model description and performance for present climate, *Clim. Dyn.*, *16*(1), 1–17, doi:10.1007/PL00007919.

Pierazzo, E., D. A. Kring, and H. J. Melosh (1998), Hydrocode simulation of the Chicxulub impact event and the production of climatically active gases, *J. Geophys. Res.*, *103*(E12), 28,607–28,625, doi:10.1029/98JE02496.

Pierazzo, E., A. N. Hahmann, and C. Sloan (2003), Chicxulub and climate: Radiative perturbations of impact-produced S-bearing gases, *Astrobiology*, *3*(1), 99–118, doi:10.1089/153110703321632453.

Pope, K. O. (2002), Impact dust not the cause of the Cretaceous-Tertiary mass extinction, *Geology*, *30*(2), 99–102, doi:10.1130/0091-7613(2002)030<0099:IDNTCO>2.0.CO;2.

Pope, K. O., K. H. Baines, A. C. Ocampo, and B. A. Ivanov (1994), Impact winter and the Cretaceous/Tertiary extinctions: Results of a Chicxulub asteroid impact model, *Earth Planet. Sci. Lett.*, *128*(3–4), 719–725, doi:10.1016/0012-821X(94)90186-4.

Pope, K. O., K. H. Baines, A. C. Ocampo, and B. A. Ivanov (1997), Energy, volatile production, and climatic effects of the Chicxulub Cretaceous/Tertiary impact, *J. Geophys. Res.*, *102*(E9), 21,645–21,664, doi:10.1029/97JE01743.

Renne, P. R., A. L. Deino, F. J. Hilgen, K. F. Kuiper, D. F. Mark, W. S. Mitchell, L. E. Morgan, R. Mundil, and J. Smit (2013), Time scales of critical events around the Cretaceous-Paleogene boundary, *Science*, *339*, 684–687, doi:10.1126/science.1230492.

Renne, P. R., C. J. Sprain, M. A. Richards, S. Self, L. Vanderkluysen, and K. Pande (2015), State shift in Deccan volcanism at the Cretaceous-Paleogene boundary, possibly induced by impact, *Science*, *350*(6256), 76–78, doi:10.1126/science.aac7549.

Royer, D. L. (2006), CO_2-forced climate thresholds during the Phanerozoic, *Geochim. Cosmochim. Acta*, *70*(23), 5665–5675, doi:10.1016/j.gca.2005.11.031.

Royer, D. L., M. Pagani, and D. J. Beerling (2012), Geobiological constraints on Earth system sensitivity to CO_2 during the Cretaceous and Cenozoic, *Geobiology*, *10*(4), 298–310, doi:10.1111/j.1472-4669.2012.00320.x.

Schmidt, G. A., et al. (2014), Using palaeo-climate comparisons to constrain future projections in CMIP5, *Clim. Past*, *10*, 221–250, doi:10.5194/cp-10-221-2014.

Schoene, B., K. M. Samperton, M. P. Eddy, G. Keller, T. Adatte, S. A. Bowring, S. F. R. Khadri, and B. Gertsch (2015), U-Pb geochronology of the Deccan Traps and relation to the end-Cretaceous mass extinction, *Science*, *347*(6218), 182–184, doi:10.1126/science.aaa0118.

Schulte, P., et al. (2010), The Chicxulub asteroid impact and mass extinction at the Cretaceous-Paleogene boundary, *Science*, *327*(5970), 1214–1218, doi:10.1126/science.1177265.

Sepúlveda, J., J. E. Wendler, R. E. Summons, and K.-U. Hinrichs (2009), Rapid resurgence of marine productivity after the Cretaceous-Paleogene mass extinction, *Science*, *326*(5949), 129–132, doi:10.1126/science.1176233.

Sewall, J. O., R. S. W. van de Wal, K. van der Zwan, C. van Oosterhout, H. A. Dijkstra, and C. R. Scotese (2007), Climate model boundary conditions for four Cretaceous time slices, *Clim. Past*, *3*(4), 647–657, doi:10.5194/cp-3-647-2007.

Vellekoop, J., A. Sluijs, J. Smit, S. Schouten, J. W. H. Weijers, J. S. Sinninghe Damsté, and H. Brinkhuis (2014), Rapid short-term cooling following the Chicxulub impact at the Cretaceous-Paleogene boundary, *Proc. Natl. Acad. Sci. U.S.A.*, *111*(21), 7537–7541, doi:10.1073/pnas.1319253111.

Vellekoop, J., J. Smit, B. van de Schootbrugge, J. W. H. Weijers, S. Galeotti, J. S. Sinninghe Damsté, and H. Brinkhuis (2015), Palynological evidence for prolonged cooling along the Tunisian continental shelf following the K–Pg boundary impact, *Palaeogeogr. Palaeoclimatol. Palaeoecol.*, *426*, 216–228, doi:10.1016/j.palaeo.2015.03.021.

Vellekoop, J., S. Esmeray-Senlet, K. G. Miller, J. V. Browning, A. Sluijs, B. van de Schootbrugge, J. S. Sinninghe Damsté, and H. Brinkhuis (2016), Evidence for Cretaceous-Paleogene boundary bolide impact winter conditions from New Jersey, USA, *Geology*, *44*(8), 619–622, doi:10.1130/G37961.1.

White, R., and A. Saunders (2005), Volcanism, impact and mass extinctions: Incredible or credible coincidences?, *Lithos*, *79*, 299–316, doi:10.1016/j.lithos.2004.09.016.

Wilde, P., and W. B. N. Berry (1986), The role of oceanographic factors in the generation of global bio-events, *Lect. Notes Earth Sci.*, *8*, 75–91, doi:10.1007/BFb0010185.

Zachos, J. C., M. A. Arthur, and W. E. Dean (1989), Geochemical evidence for suppression of pelagic marine productivity at the Cretaceous/Tertiary boundary, *Nature*, *337*(6202), 61–64, doi:10.1038/337061a0.